

<sup>1</sup>

<sup>2</sup> **Antiproton to Proton Ratio with the Alpha  
3 Magnetic Spectrometer on the International  
4 Space Station**

<sup>5</sup> Von der Fakultat fur Mathematik, Informatik und Naturwissenschaften der RWTH Aachen  
<sup>6</sup> University zur Erlangung des akademischen Grades eines Doktors der Naturwissenschaften  
<sup>7</sup> genehmigte Dissertation

<sup>8</sup> vorgelegt von

<sup>9</sup> **Sichen Li, M.Sc.**

<sup>10</sup> aus

<sup>11</sup> Xi'an

<sup>12</sup> Berichter: Univ.-Prof. Dr. rer. nat. Stefan Schael

<sup>13</sup> Jun.-Prof. Dr. rer. nat. Philipp Mertsch

<sup>14</sup> Tag der mundlichen Prufung: 20. Oktober 2022

<sup>15</sup> Diese Dissertation ist auf den Internetseiten der Universitatsbibliothek online verfugbar.

## CONTENTS

57	1 : INTRODUCTION . . . . .	1
58	2 : COSMIC RAYS . . . . .	3
59	2.1 Cosmic Rays . . . . .	3
60	2.2 Source of cosmic rays . . . . .	6
61	2.3 Propagations . . . . .	7
62	2.4 Cosmic antiprotons measurement . . . . .	11
63	3 : AMS-02 EXPERIMENT . . . . .	14
64	3.1 Experiment Overview . . . . .	14
65	3.2 Transition Radiation Detector . . . . .	17
66	3.3 Tracker . . . . .	20
67	3.4 TOF . . . . .	24
68	3.5 RICH . . . . .	25
69	3.6 ECAL . . . . .	27
70	3.7 ACC . . . . .	29
71	4 : ANALYSIS . . . . .	31
72	4.1 Data Selection . . . . .	31
73	4.2 Charge confusion estimator . . . . .	37
74	4.3 TRD estimator . . . . .	42
75	4.4 Template Fit . . . . .	45
76	4.5 Effective Acceptance . . . . .	53
77	4.6 Measuring Time . . . . .	57
78	4.7 Trigger Efficiency . . . . .	66
79	4.8 Unfolding . . . . .	70

80	4.9 Systematic Uncertainty . . . . .	75
81	5 : RESULTS . . . . .	78
82	5.1 Time Averaged Result . . . . .	78
83	5.2 Time Dependent Result . . . . .	80
84	6 : SUMMARY . . . . .	85
85	A : APPENDIX - INPUT VARIABLES FOR CHARGE CONFUSION . .	86
86	B : APPENDIX - YYY . . . . .	88
87	Acknowledgments . . . . .	89
88	BIBLIOGRAPHY . . . . .	90

<sub>89</sub> CHAPTER 1

<sub>90</sub> INTRODUCTION

<sub>91</sub> The story of cosmic rays began in 1912, a balloon experiment carried out by Victor Hess  
<sub>92</sub> showed a significant rise in the ionization rate with the altitude going up [1] , which is  
<sub>93</sub> confirmed to be caused by cosmic rays then. The discovery of cosmic rays opens a new  
<sub>94</sub> window to explore our universe except astronomical observations. Since then, enormous  
<sub>95</sub> effort have been put in to identify the components of cosmic rays and to measure the flux  
<sub>96</sub> in large energy scale. Due to the unique high energy level of cosmic rays can reach, the  
<sub>97</sub> cosmic rays provide a possibility to study the high energy particle above TeV, which is the  
<sub>98</sub> maximum energy level for collider physics can reach.

<sub>99</sub> Before the particle accelerator was invented, the main source to study high energy particles  
<sub>100</sub> was through cosmic rays. The positron was firstly found in 1932 by Carl David Anderson  
<sub>101</sub> in cosmic rays [2] . This is the beginning of discovering antimatters. After that, particle  
<sub>102</sub> accelerator made great improvement and antiproton was discovered in 1955 by Emilio Segrè  
<sub>103</sub> and Owen Chamberlain at the Bevatron particle accelerator [3] . The presence of antiproton  
<sub>104</sub> in cosmic rays was firstly confirmed in 1979 by two balloon experiments. Since then, the  
<sub>105</sub> effort to studying cosmic antiprotons never stop.

<sub>106</sub> Due to the earth atmosphere, the cosmic antiprotons can only be measured either in balloon  
<sub>107</sub> experiments or space spectrometers. In this thesis, Data collected by the AMS-02 experiment  
<sub>108</sub> is used to determine the antiproton to proton flux ratio, including time averaged analysis and

109 time dependent analysis. The AMS-02 experiment was installed on the International Space  
110 Station in May 2011, which has a permanent magnet to distinguish the sign of rigidity of  
111 particles. Up to May 2021, 10 years cosmic rays data have been collected, antiproton signals  
112 can be identified from bunch of cosmic ray events.

113 Before the AMS-02 experiment, there was no continuous measurement of cosmic antiprotons.  
114 Some balloon experiments measured cosmic antiprotons in several flights. Space spectrome-  
115 ter PAMELA also only published time averaged antiproton result. Since AMS-02 have been  
116 monitoring cosmic rays continuously up to today, the time dependent antiproton analysis is  
117 possible to be done with the data collected. In this thesis, the time dependent antiproton to  
118 proton flux ratio is presented in 6 Bartels Rotations time resolution, which is the first time  
119 the solar modulation's effect on cosmic antiprotons is shown.

120 In Chapter 2, a general picture about cosmic rays will be shown. In Chapter 3 the details of  
121 all sub-detectors in AMS-02 experiment will be given. Chapter 4 will present the antiproton  
122 analysis techniques used in this analysis. In Chapter 5 the result of antiproton to proton  
123 flux ratio with 10 years data will be shown, also the time dependent antiproton to proton  
124 flux ratio with time resolution of 6 Bartels Rotations. Chapter 6 will give a summary and  
125 conclusion on this thesis.

<sub>126</sub> CHAPTER 2

<sub>127</sub> COSMIC RAYS

<sub>128</sub> 2.1. Cosmic Rays

<sub>129</sub> The curiosity to explore the unknown world is the initial and forever driver for human being.

<sub>130</sub> Limited by the scale of human activity, up to today the highest energy can be reached though

<sub>131</sub> manmade particle accelerator is TeV level. To study the beyond, our universe itself can be

<sub>132</sub> served as a tool, namely, "Universe is the ultimate laboratory for particle physics."

<sub>133</sub> The spectra of cosmic rays cover a incredibly large range. The measured cosmic rays flux

<sub>134</sub> can vary in 31 orders of magnitude, which is the scale of visible universe compared to

<sub>135</sub> human hair. The measured energy of cosmic rays can go up to ZeV level ( $10^{21}$  eV), which is

<sub>136</sub> impossible to generate from human made facilities currently. The large dynamic range can

<sub>137</sub> be seen in figure 2.1(a). As shown in this figure, the cosmic rays flux follows a power law,

<sub>138</sub> and the spectral index  $\gamma \approx 2.7$ . Below  $10^{10}$  eV (10 GeV) the flux is lower than power law

<sub>139</sub> extrapolation due to the deflection caused by the solar magnetic field. Around  $4 \times 10^{18}$  eV

<sub>140</sub> (4 EeV) the spectrum index steeps to around 3.1, which is called "knee". Above this energy

<sub>141</sub> level the spectrum index backs to around 2.7, the transition period is called "ankle". In

<sub>142</sub> addition, theoretically no cosmic ray can be higher than  $5 \times 10^{19}$  eV (50 EeV), the upper limit

<sub>143</sub> is called GZK limit [4, 5], while some experiment appeared to detect cosmic ray with higher

<sub>144</sub> energy. This brings a unsolved puzzle to be investigated. These features and observations

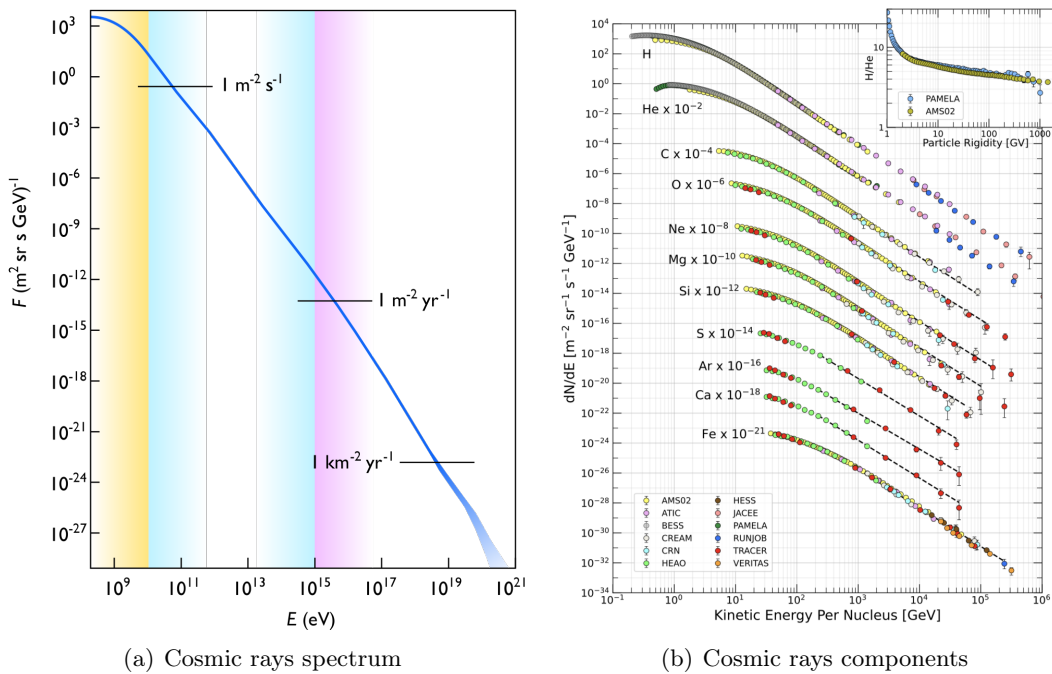


Figure 2.1: Cosmic ray spectra [6]

145 are important to understand the sources of cosmic rays and also the propagation of cosmic  
 146 rays.

147 Our earth is constantly bombarded by subatomic particles. Due to the earth atmosphere,  
 148 the ground based cosmic rays measurements can only measure cascaded cosmic rays. To  
 149 measure the cosmic rays directly, detectors have to be placed above atmosphere. AMS-02  
 150 experiment is conducted on the ISS, which is at around 417 km height, therefore it can  
 151 precisely measure the cosmic rays without consideration of interactions with atmosphere.

152 There are two kinds of cosmic rays: primary and secondary. Primary cosmic rays are  
 153 produced in astrophysical sources, while the secondary cosmic rays are from the interaction  
 154 between primary cosmic rays and interstellar medium. Primary cosmic rays have protons,  
 155 electrons, He et al. Secondary cosmic rays have positrons, antiprotons, Li, Be et al.

156 Cosmic rays consist of many components. For primary cosmic rays protons takes up around  
 157 89%, 10% are helium nuclei, and around 1% are heavy elements. In figure 2.1(b) the fluxes

158 of different cosmic rays components are given. A universal power law spectrum is observed  
 159 in all kinds of cosmic rays, which supports the assumption of a general electro-magnetic  
 160 acceleration mechanism, though the small differences are still need to be investigated. With  
 161 the efforts of different measurements, the cosmic ray components fluxes have been measured  
 162 in a large range.

163 In figure 2.2, the galactic cosmic rays abundances compared with solar system ones are  
 164 shown. In general, the matching between galactic cosmic rays and abundance in solar system  
 165 is very good. The reduction of cosmic hydrogen and helium are due to solar magnetic field.  
 166 Because the spallation and interaction reactions in cosmic rays, the CNO nuclei would break  
 167 into lower mass element, namely Li, Be, and B. This explains the over-abundance of Li, Be  
 168 and B and less abundance of CNO in cosmic rays compared to solar system.

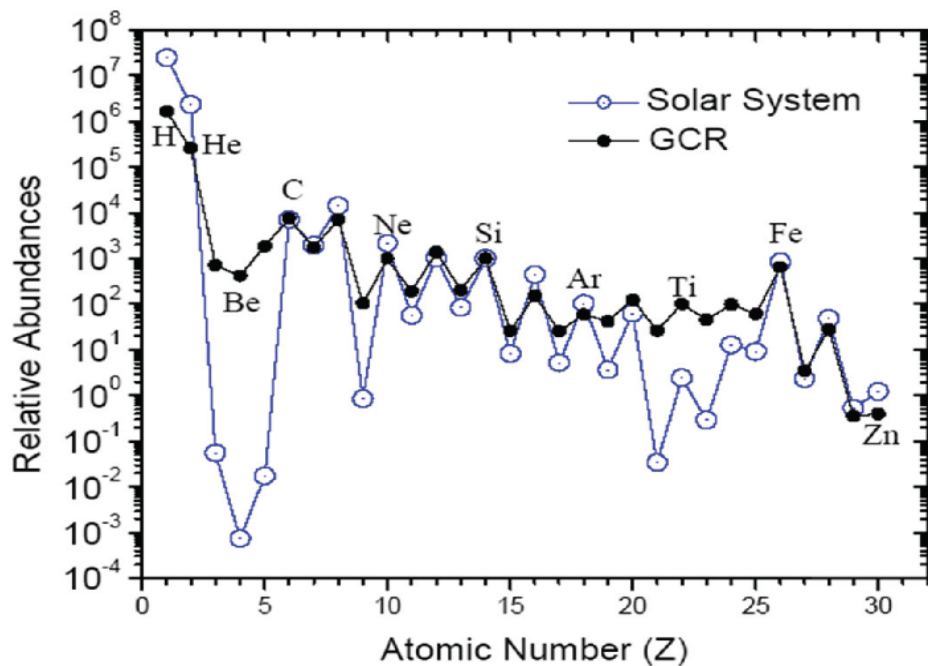


Figure 2.2: Element abundance of cosmic rays [7]

169 **2.2. Source of cosmic rays**

170 Traditionally, the supernova remnant (SNR) are considered to be the main sources of cos-  
171 mic rays. This idea was firstly suggested by Baade and Zwicky in 1934 [8] . Apart from  
172 SNR, some other sources can also contribute to cosmic rays production, like pulsars or dark  
173 matters. Therefore, precisely measuring cosmic ray flux certainly is a probe to understand  
174 the sources of cosmic rays.

175 The supernova is a stellar explosion event that can expel several solar masses of material  
176 with very high speed. There are mainly two mechanisms of supernova [9] : A white dwarf  
177 reaches the Chandrasekhar limit and then triggered into a nuclear fusion; or a gravitational  
178 core collapse of a massive star. These two both can accelerate ejected materials into a few  
179 percent level of speed of light. The ejected material is traveling faster than the speed of  
180 sound in the ISM and therefore creates a expanding shock wave which could sweep the shell  
181 of gas and dust to create a "supernova remnant" [10] , this can heat the plasma above  
182 millions of Kelvins.

183 Charged particles can be absorbed into the supernova remnant and be confined in it. In this  
184 process, charged particles gain energy and be accelerated while trapped in the supernova  
185 remnant until their energy are large enough to escape from it. The acceleration mechanisms  
186 are called "First Order Fermi Mechanism" and "Second Order Fermi Mechanism". The first  
187 one describes the particles crossing the front shock repeatedly and gain energy [11] . The  
188 second one describes the acceleration from the particle collisions with magnetic clouds in  
189 the interstellar medium [12] . These acceleration processes in the supernova remnant would  
190 eventually lead to a power law energy spectrum in cosmic ray spectrum.

191 Apart from the SNR, pulsars can also contribute high energy cosmic rays. Pulsars are  
192 rapidly rotating neutron stars with strong magnetic field. Area surrounding pulsar are  
193 called pulsar wind nebula (PWN). In PWN, by pair production the electrons and positrons  
194 can be produced [13, 14] . Through centrifugal mechanism of acceleration, the shock of PWN

195 with surrounding matters can accelerate charge particles into high energy range [15, 16] .  
196 This is regarded as another important contribution in high energy electron and positron  
197 spectrum.

198 Pulsars can produce positrons while antiprotons can not be produced by pulsars [17, 18] ,  
199 therefore, the contribution of cosmic antiprotons can only be from the interactions between  
200 primary cosmic rays and ISM. If additional cosmic antiproton is observed, other sources of  
201 antiprotons like dark matters can be checked [19, 20, 21] . So in general by measuring the  
202 antiproton spectrum precisely, the sources of cosmic antiprotons can be investigated.

### 203 2.3. Propagations

#### 204 2.3.1. Cosmic ray propagating in the galaxy

205 When the accelerated cosmic rays leave the SNR, they would travel through the Galaxy  
206 and then interact with ISM, this produce secondary cosmic rays. By hadronic production,  
207 antiprotons can be generated. Positron and electron lose their energy by bremsstrahlung.  
208 Due to the charge of cosmic rays, they are scattered on the magneto-hydrodynamic waves,  
209 this deflects the trajectory of cosmic rays from straight line. In big picture, the path of  
210 cosmic rays can be described by a diffusion process, this diffusion effect together with other  
211 physics effects can be quantitatively described by transport equation [22] :

$$\frac{\partial \psi(\vec{r}, p, t)}{\partial t} = q(\vec{r}, p, t) + \vec{\nabla} \cdot (D_{xx} \vec{\nabla} \psi - \vec{V} \psi) + \frac{\partial}{\partial p} p^2 D_{pp} \frac{\partial}{\partial p} \frac{1}{p^2} \psi - \frac{\partial}{\partial p} \left[ \dot{p} \psi - \frac{p}{3} (\vec{\nabla} \cdot \vec{V}) \psi \right] - \frac{1}{\tau_f} \psi - \frac{1}{\tau_r} \psi \quad (2.1)$$

212 where, the  $\psi(\vec{r}, p, t)$  is the density of cosmic rays at point  $\vec{r}$  with momentum  $p$ . The different  
213 terms can be correspondent to different physics processes and are explained here:

- 214 •  $q(\vec{r}, p, t)$  denotes the source term, this include the primary sources, and the contribu-

215 tions from spallation and decay process.

216 •  $D_{xx}$  is the spatial diffusion coefficient, which shows the scattering with the magneto-  
217 hydrodynamic waves.

218 •  $\vec{V}$  is the convection velocity. The galactic wave bring an additional convective trans-  
219 port and this can lead to adiabatic energy losses.

220 •  $D_{pp}$  is the momentum diffusion coefficient. Apart from the spatial diffusion process,  
221 charged particles in random traveling in magneto- hydrodynamic waves can cause the  
222 stochastic re-acceleration process, and this process can be described by the momentum  
223 diffusion coefficient.

224 •  $\vec{\nabla} \cdot \vec{V}$  denotes the adiabatic momentum change, this term is the result from inhomog-  
225 eneous gas with magnetic field scattering the cosmic rays.

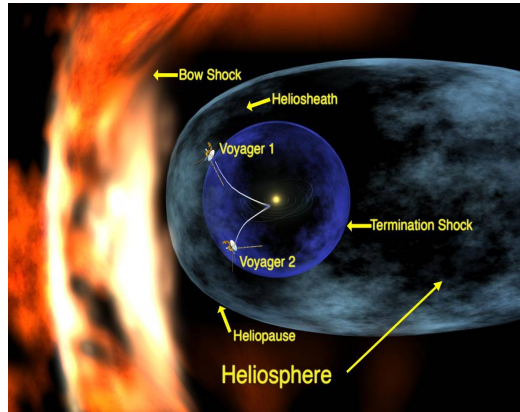
226 •  $\tau_f$  and  $\tau_r$  are time scale of fragmentation and decay respectively.

227 Foe each particle type a propagation equation is used dedicatedly, this lead to a very com-  
228 plex system of different differential equations. To solve these equations analytically is very  
229 hard, therefore numerical calculation is more practical, like Monte-Carlo based approach.  
230 Specifically, some software tools are widely used to get the solution, like GALPROP [23] ,  
231 USINE [24] , and DRAGON [25] .

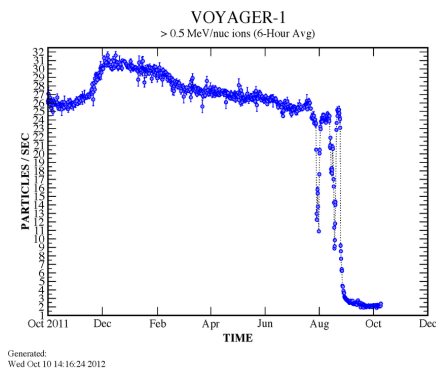
232 Except from numerical solution, with the basic assumption of galaxy is a box where particles  
233 can freely propagate without interaction but only elastic scattering, the transport equation  
234 can be simplified to:

$$\frac{\partial \psi(\vec{r}, p, t)}{\partial t} = \psi_0(p) \cdot \delta(t) - \frac{\psi(p, t)}{\tau_{esc}} \quad (2.2)$$

235 where  $\tau_{esc}$  is escape time which represents the constant escape probability. This is called  
236 Leaky box model and the solution of the equation is  $\psi(p, t) = \psi_0(p) \exp(-\frac{t}{\tau_{esc}})$ .



(a) Heliosphere. Credit: NASA/Walt Feimer



(b) Particle rate detected by Voyager1 (October 2011 through October 2012). [31]

Figure 2.3: Heliosphere at edge of solar system

### <sup>237</sup> 2.3.2. Cosmic ray propagating in the heliosphere

<sup>238</sup> The sun is continuously ejecting the charge particles from its upper atmosphere when the  
<sup>239</sup> energy of those particles reach the escape limit, those charged particles are called "solar  
<sup>240</sup> wind" [26, 27]. The solar wind are charged so they are embedded interplanetary magnetic  
<sup>241</sup> field [28]. With these embedded magnetic field, the solar wind plasma spread with a typical  
<sup>242</sup> speed of 400 m/s, faster than the speed of magnetosonic wave therefore it's supersonic. After  
<sup>243</sup> traveling for some distance and encountering the interstellar medium, the speed of solar wind  
<sup>244</sup> abruptly decelerate and become subsonic. This create a termination shock, which is called  
<sup>245</sup> "Heliosphere" [29]. See figure 2.3(a) for illustration. In 2012, Voyager 1 probe became the  
<sup>246</sup> first spacecraft to cross the heliosphere [30]. The solar particle dramatically decreased after  
<sup>247</sup> reaching the end of the heliosphere, see figure 2.3(b).

<sup>248</sup> When galactic cosmic rays enter the solar system, they would travel through the heliosphere  
<sup>249</sup> first. Since the solar wind are released from corona, which has a cycle of 22 years for solar  
<sup>250</sup> activity [32]. The physical status of heliosphere also varies in a 22 years cycle. After passing  
<sup>251</sup> the heliosphere, the cosmic rays are modulated by this effect and therefore show a closed  
<sup>252</sup> variation in 22 years. The solar cycle is counted from 1755 and now we are in the beginning

253 of solar cycle 25. [33, 34]

254 In figure 2.4, the different ground based measured cosmic neutron variations with time  
255 are shown. Since the sunspot numbers are correspondent to the sun activity, they are  
256 anti-correlated with the measured cosmic rays. By measuring the cosmic rays in long time  
257 period, the impact from solar activities would be seen. Up to today, the long time continuous  
258 measurement only have been done through dominant cosmic rays like protons or the cascaded  
259 production like neutrons. For the rare component like antiproton, there is no continuous  
260 measurement about it. Since AMS-02 experiment has been collecting cosmic data for 10  
261 years, the first time dependent antiproton result is possible to achieve.

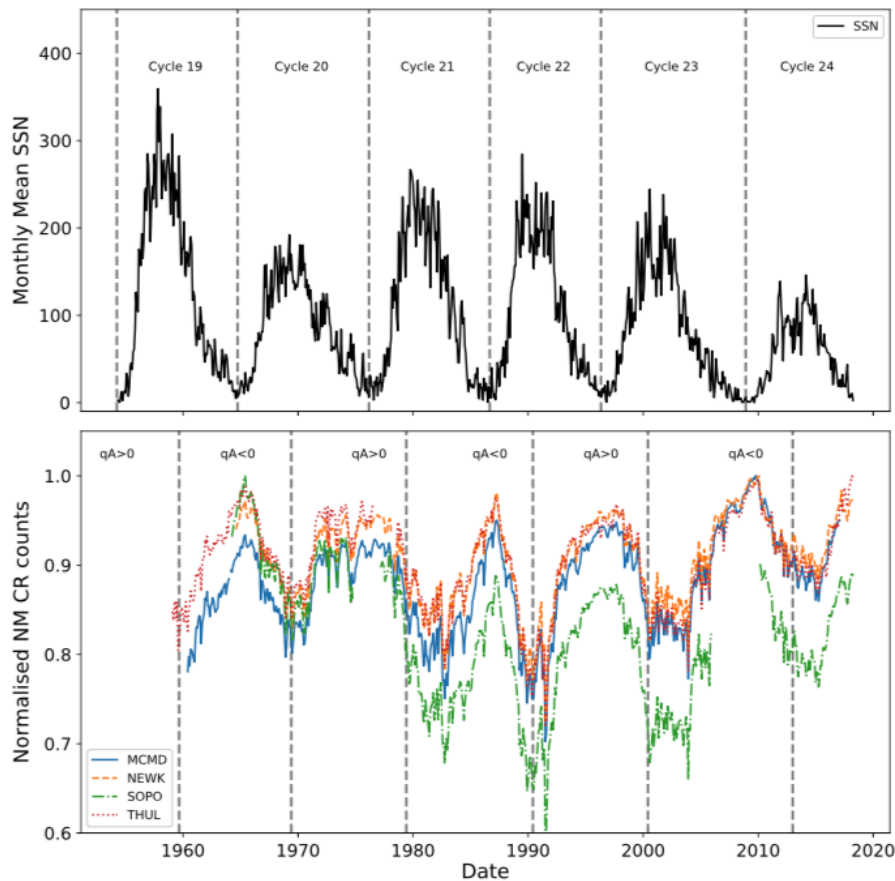
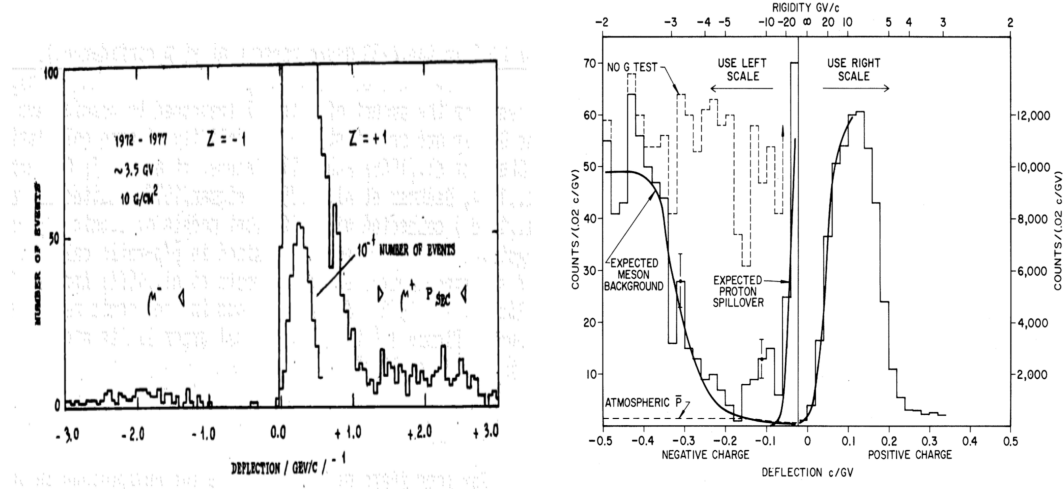


Figure 2.4: Ground based neutron monitors [35]



(a) The balloon flight experiment carried out by Bogomolov et al. in 1979. [36] (b) The balloon flight experiment carried out by Golden et al. in 1979. [37]

Figure 2.5: First two cosmic antiproton measurements

## 2.4. Cosmic antiprotons measurement

Cosmic ray was discovered in 1912 [1], antiproton was discovered in 1955 [3], the first measurements of cosmic antiproton component were in 1979 [36, 37]. In 1979, two pioneering balloon flight experiments published their results about cosmic antiprotons independently. The first one was carried out by Bogomolov et al. and the data taking was from 1972 to 1977 by three individual flights, the residual air was  $11 \text{ g/cm}^2$  and the result showed two candidates of cosmic antiprotons in kinetic energy range 2-5 GeV. The second was carried out by R. L. Golden et al. and data taking was from June 21 to June 22 in 1979, the location was Palestine, Texas and the residual air in this area was  $5.4 \text{ g/cm}^2$ . The spectrometer had a superconducting-magnet and the group reported 46 antiproton candidates from 5.6 to 12.5 GV. In figure 2.5, the cosmic antiproton candidates in those two experiments are shown.

After decades of effort, many cosmic rays experiments published results about cosmic antiprotons. In balloon flight experiments, the representative program is the BESS experiment, which had 9 successful flight campaigns since 1993. The incarnation program are BESS-Polar I & II [38, 39] carried out in 2004 and 2008 respectively and both the two flights

277 measured the cosmic antiprotons [40, 41]. In the final result from BESS-Polar II experi-  
 278 ment, the group used data taken from Dec 2007 to Jan 2008, which was correspondent to a  
 279 solar minimum, and report measurement of 7886 cosmic antiprotons in kinetic energy range  
 280 from 0.17 to 3.5 GeV [41]. Figure 2.6 shows the antiproton signals in TOF Beta versus  
 281 Rigidity space in the flight of BESS-Polar II.

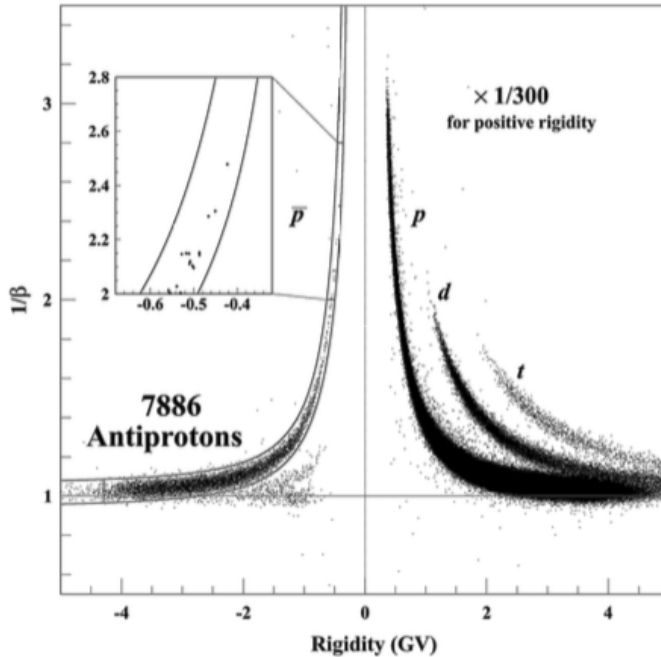


Figure 2.6: Cosmic antiprotons measured by BESS-Polar II [41]

282 Due to the height of balloon flight experiments, the correction of residual air has to be  
 283 considered into calculation, while in space the residual air is ignorable, so this brings to  
 284 another solution, that is to place a spectrometer in space. The first satellite based cosmic  
 285 antiproton measurement was from PAMELA detector. PAMELA mission was from June  
 286 2006 to February 2016, the float altitude was between 350 km and 610 km. Floating period  
 287 was 94 mins and the host satellite was Resurs-DK1 [42]. The PAMELA group published  
 288 several antiproton results and the last one was in 2012 [43, 44, 45], the measured energy  
 289 was up to 350 GeV [45]. This result shows a relatively flat antiproton to proton flux ratio  
 290 in high energy range, which is different from the traditional prediction of cosmic antiprotons

<sup>291</sup> from purely secondary production. In 2016 AMS-02 experiment published its first result on  
<sup>292</sup> cosmic antiprotons, this extend the energy range up to 450 GV with first 4 years collected  
<sup>293</sup> cosmic rays data [46]. The details of AMS-02 experiment will be shown in next chapter.

294 CHAPTER 3

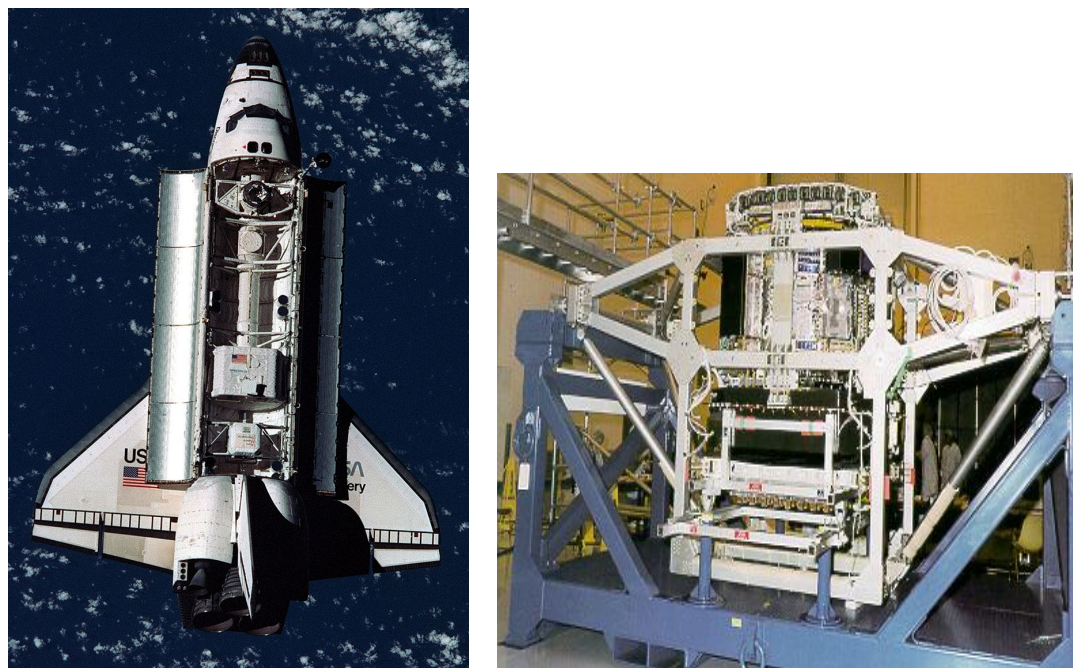
295 AMS-02 EXPERIMENT

296 3.1. Experiment Overview

297 The Alpha Magnetic Spectrometer (AMS) program was proposed by Nobel Laurent Prof.  
298 Samuel Ting from MIT in 1995 and was accepted then [47] . The goal of the experiment  
299 is to measure the antimatter in cosmic rays and provide precise measurement of fluxes for  
300 different components of cosmic rays, which is crucial to understand the sources of cosmic  
301 rays and the basic propagation model of cosmic rays. [48]

302 To test the feasibility of the particle spectrometer in space, a prototype called AMS-01 was  
303 designed, which was a simplified version of the final experiment, see figure 3.1(b). The  
304 test flight was conducted in 1998 in space shuttle flight STS-91 [49] , see figure 3.1(a). By  
305 collecting cosmic rays data for 10 days, the test flight was very successful to prove that  
306 putting a spectrometer in space is possible.

307 After several years of construction and test, the AMS-02 detectors were launched by space  
308 shuttle Endeavour in STS 134 mission from Kennedy Space Center on 16 May 2011. Three  
309 days later, the detector was installed on the upper Payload Attach Point (S3) of ISS and  
310 began data taking. Figure 3.2 shows the location of AMS-02 on the ISS.



(a) AMS-01 test flight in STS 91 space shuttle flight [50] (b) AMS-01 detector installed in the support structure. credit: AMS-01 brochure

Figure 3.1: The AMS-01 experiment



Figure 3.2: AMS-02 detector on the ISS. Image modified from [51]

311 The AMS-02 experiment has a size of  $5\text{ m} \times 4\text{ m} \times 3\text{ m}$ , weight of  $7.5\text{ t}$  [52]. It has a  
 312 permanent magnet with  $0.14\text{ T}$ , combined with 9 silicon tracker layers mostly in the middle  
 313 of the detector, the rigidity can be measured. Within the magnet, the Anti-coincidence  
 314 counters is used as a veto system to reject particles coming from side. At the relative top  
 315 of the experiment, there is a transition radiation detector, which can distinguish light and  
 316 heavy particles. Above and below the magnet, there are two time of flight systems installed  
 317 to provide trigger and measurement of velocity and charge. Below the lower part of TOF, a  
 318 ring imaging cherenkov detector is located so the velocity of particle can be measured. At  
 319 the bottom of the detector, there is a electromagnetic calorimeter which can measure the  
 320 energy of particles. The geometry of all the sub-detectors is illustrated in figure 3.3.

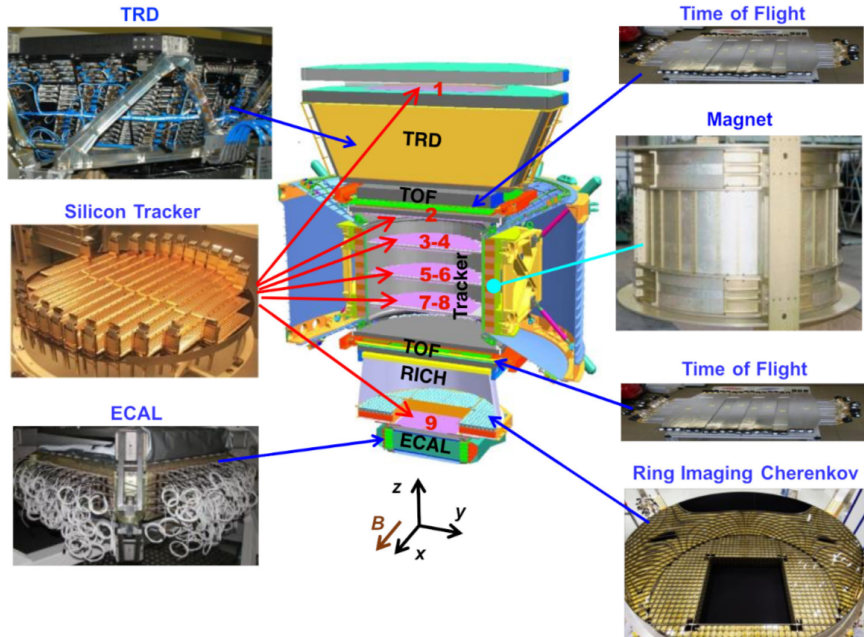


Figure 3.3: Schematic view of AMS-02 detectors. [53]

321 To make the experiment running smoothly, the experiment operation has been conducted  
 322 since the launch. The whole operations can be split into flight and underground parts. In  
 323 figure 3.4 the operation process is illustrated. The collected data is transmitted from upper  
 324 left to lower left in this figure with a clockwise sequence and the command from underground

325 to space station is follow the counterclockwise sequence.



Figure 3.4: AMS-02 operations flow [54]

### 326 3.2. Transition Radiation Detector

327 Transition Radiation Detector (TRD) can separate different particles by having different  
328 transition radiations. Transition radiation is emitted when a charged particle going through  
329 the boundary between two different media [55]. The emitted radiation is produced be-  
330 cause the different inhomogeneous solutions of Maxwell's equation of charged particle in  
331 two mediums, so the particle has to emit photon to compromise the differences. The inten-  
332 sity of emitted photon is proportional to the Lorentz factor  $\gamma$ , so for the relativistic charged  
333 particle, the characteristic energy of the radiation is X-ray. The direction is mostly forward  
334 and the angle between transition radiation and particle path is proportional to  $1/\gamma$ .

335 AMS-02 experiment has a transition radiation detector, which is placed on the top of the  
336 experiment, between tracker layer 1 and the upper TOF layer [56, 57]. The TRD has 5248  
337 proportional tubes, each one has 6 mm diameter and with maximum 2 meters length. The

338 tubes have double-layer  $72 \mu\text{m}$  kapton aluminium foil walls and at the center of tube is  $30$   
339  $\mu\text{m}$  tungsten wire. Inside the tubes there are  $\text{CO}_2$  and  $\text{Xe}$  gas mixture supplied from storage  
340 tanks ( $5 \text{ kg CO}_2$  and  $49 \text{ kg Xe}$ ). When a charged particle goes through the tube, it can  
341 ionise the  $\text{Xe}$  atom and create a avalanche of ionisation which is proportional to the energy  
342 loss of the charged particle. Then the  $\text{CO}_2$  could quench the environment and reset to the  
343 initial state. So far, no detectable leak in AMS-02 TRD gas system is observed. Due to the  
344 diffusion, the loss of  $\text{CO}_2$  is around  $0.47 \text{ g/day}$  and for  $\text{Xe}$  the loss is ignorable, this ensures  
345 that TRD can stably operate until 2035.

346 These TRD tubes are assembled in 328 modules so one module has 16 tubes. Furthermore  
347 all these modules are mounted in 20 layers, 12 layers are placed along to Y axis in middle of  
348 TRD, 4 layers are placed on top and 4 layers on bottom. In figure 3.5, the real size of TRD  
349 is shown when its construction was completed in Aachen.

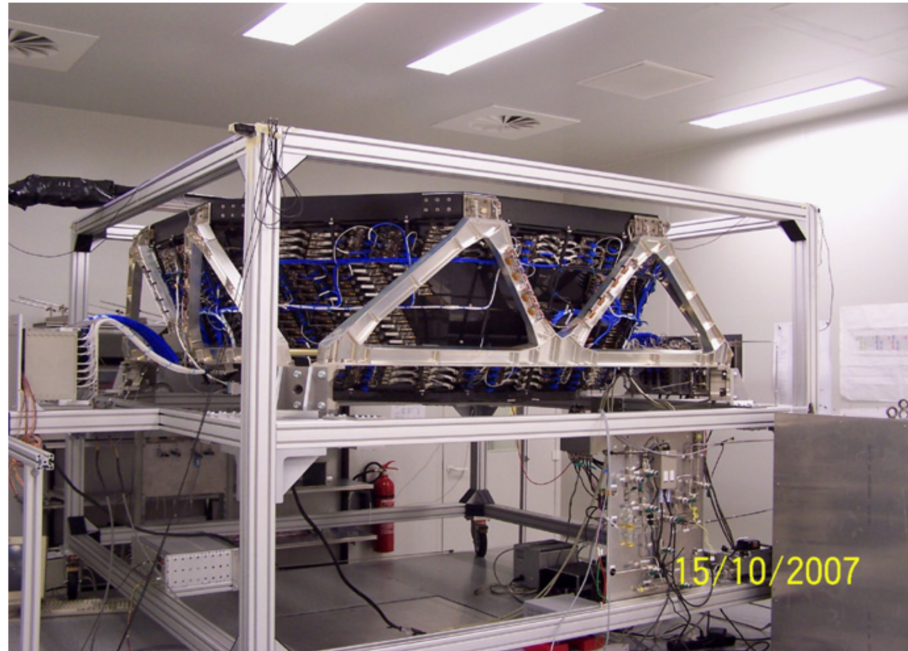


Figure 3.5: TRD construction completed in RWTH Aachen. [58]

350 In figure 3.6, the left figure shows the response when a electron and proton going through one  
351 TRD layer. Upper part of layer is a  $20 \text{ mm}$  fleece radiator, which has  $10 \mu\text{m}$  polypropylene

352 or polyethylene fibres. Lower part of layer are straw tubes. When a relativistic charged  
 353 particle goes through radiator, transition radiation may produced. For example, after a  
 354 proton traversing the layer,  $dE/dx$  signal can be recorded, while a electron passing the  
 355 layer, also the transition radiation can be collected in straw tubes. In the right figure, the  
 356 distributions in tube collected energy for 100 GeV protons and 20 GeV electrons are shown  
 357 as an example. Due to the transition radiation emitted by electron, around 10 KeV photons  
 358 are observed.

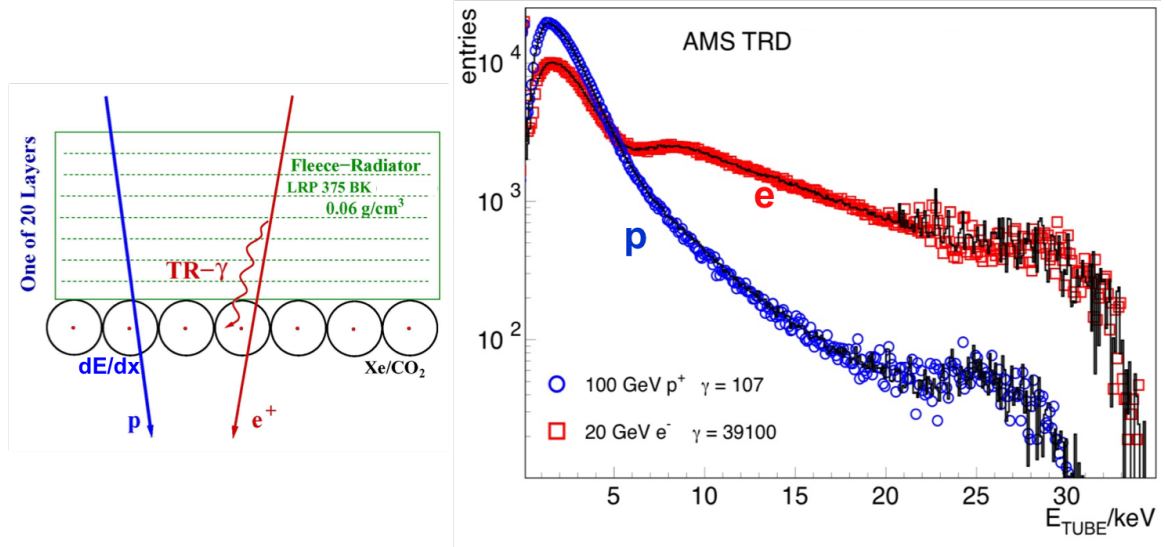


Figure 3.6: Illustration of TRD separation between electrons and protons. [54]

359 The signals from the 20 layers are combined to construct a likelihood  $\mathcal{L}$  for each particle  
 360 specie. For example, for electron and proton,  $\mathcal{L}_e$  and  $\mathcal{L}_p$  are constructed. Then according  
 361 to Neyman-Pearson lemma [59] , in the form of likelihood ratio, the separation power can  
 362 reach maximum, therefore the TRD estimator is defined as:

$$\Lambda_{TRD} = -\log\left(\frac{\mathcal{L}_A}{\mathcal{L}_A + \mathcal{L}_B}\right) \quad (3.1)$$

363 if A = electron and B = proton, then the likelihood is "TRDElectronProtonLikelihood"  
 364 which provide separation power for electron and proton. In figure 3.7, the distribution of

365 electron and proton are shown in TRD estimator, the two kinds of particles can be very well  
366 separated as shown in this figure.

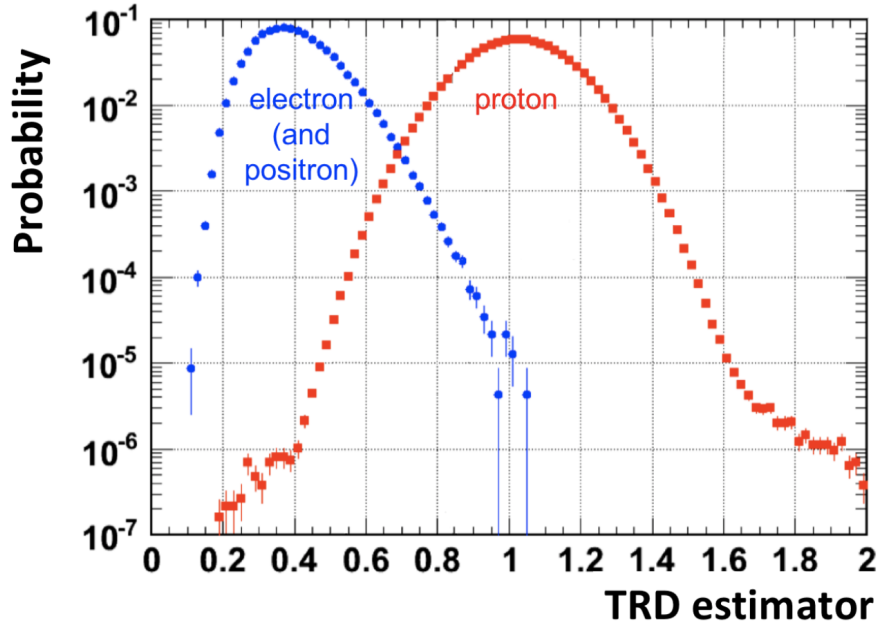


Figure 3.7: Separation for electrons and protons in TRD estimator. [54]

### 367 3.3. Tracker

368 To measure the sign of rigidity, a silicon tracker system with a magnet is equipped in AMS-02  
369 experiment. Originally the magnet was to be a superconducting magnet with 0.8 T field [60]  
370 , but due to the thermal issue and lifetime of the experiment, the superconducting magnet  
371 was replaced by a permanent magnet [61] . The magnet used in AMS-02 experiment is  
372 a permanent magnet with 0.14 T field. The magnet has 64 Nd-Fe-B sectors arranged in  
373 cylinder shape with 0.8 m height and 1.1 m diameter inside. The produced magnet field is  
374 almost linear and the magnet field direction is defined as X direction, the vertical direction  
375 is Z direction, so the particle bending plane is YZ plane. Outside the magnet, the leaking  
376 magnet field is ignorable so the design can minimise the magnetic effect to the ISS.

377 In figure 3.8, the permanent magnet used in AMS-02 is shown. Since the magnet is same as

378 AMS-01, the magnet field of the magnet is remeasured again 2010, compared with the first  
379 measurement in 1997, the deviation is less than 1% as showed in 3.9.



Figure 3.8: Preparing for the vibration test in China Academy of Launch Vehicle Technology [54]

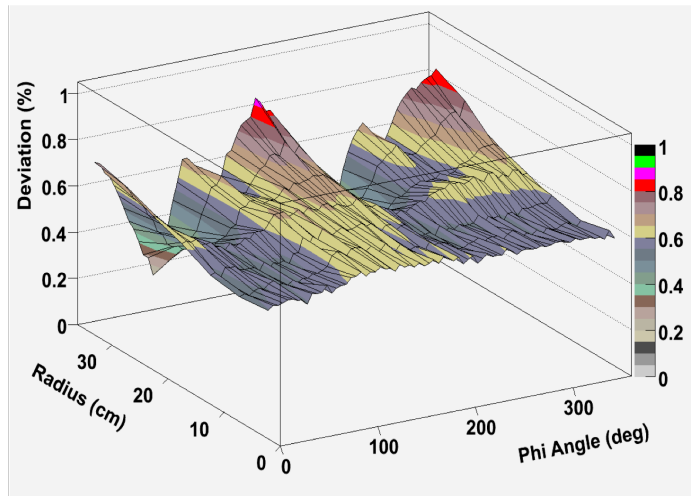


Figure 3.9: Deviation of measured magnet field between 2010 and 1997 [54]

380 With the permanent magnet, the silicon tracker can measure the charge  $Z$  and also the  
381 momentum  $p$  of the particle.

382 The tracker in AMS-02 has 9 silicon layers, the first layer is on the top of TRD, second  
383 layer is above the magnet and below the upper TOF, layer 3 to 8 are inner central layers

384 which are installed inside the permanent magnet, layer 9 is above ECAL and below RICH.  
385 In total, the all 9 layers have 2264 double sided silicon micro-strip sensors, they are arranged  
386 into 192 ladders [62, 63]. The summed up active measurement area is  $6.75 \text{ m}^2$ . For signal  
387 readout, each ladder has 1024 readout strips, 640 on the p-side and 384 on the n-side, so in  
388 total 196608 readout strips are reading out the signals.

389 The double sided silicon micro-strip sensor has size of  $41.360 \times 72.045 \text{ mm}^2 \times 300 \mu\text{m}$ .  
390 When a particle goes through the sensor, it would create electron hole pairs in middle. The  
391 created electrons would drift towards the n-side and hole would towards the p-side, so both  
392 the X and Y side position measurements are provided. Figure 3.10 illustrate the process.  
393 The design of the tracker ensure that in bending direction and non-bending direction the  
394 resolution are around  $10 \mu\text{m}$  and  $30 \mu\text{m}$ . Also, since the signal is proportional to  $dE/dX$   
395 measurement, the charge measurement of each layer can be obtained. The charge resolution  
396 of the inner tracker layers is  $\Delta Z = 0.05$  for charge one particle.

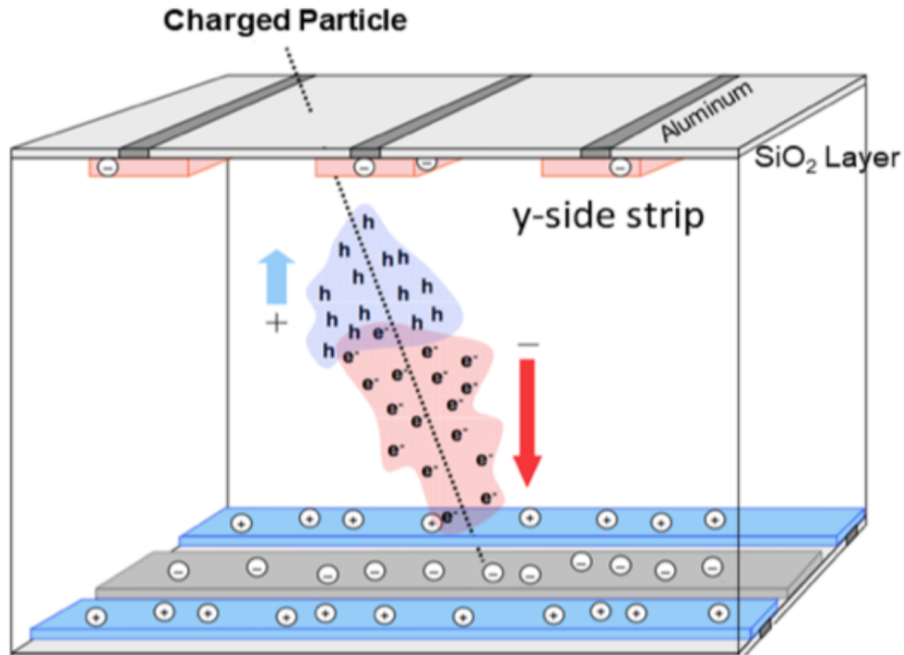


Figure 3.10: Drift of electron hole pair in silicon sensor. [54]

397 For the inner tracker layer, the positions are aligned with 20 IR laser beams with sub-micron

398 measurement [64, 65] . Layer 1 and 9 position alignment are done with fresh 2 minutes cosmic  
 399 rays, this gives  $5 \mu\text{m}$  and  $6 \mu\text{m}$  variations for layer 1 and 9 respectively.

400 Before the launch of AMS-02, the whole detector was tested at CERN SPS with proton  
 401 beam of 180 and 400 GeV, positron, electron and pion beam of 10 to 290 GeV. These exten-  
 402 sive calibration data give precise measurement to determine the tracker rigidity resolution  
 403 function and also make the comparison and calibration with MC possible. Figure 3.11 shows  
 404 the 400 GeV proton calibration data and MC comparison, a good match between these two  
 405 is observed.

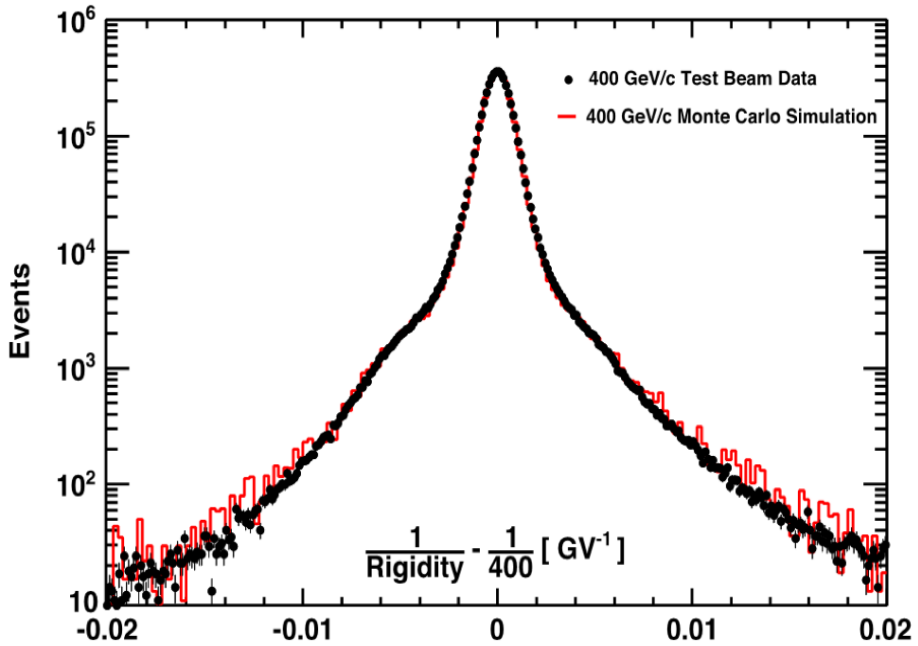


Figure 3.11: 400 GeV proton beam test result and MC comparison. [54]

406 The electronics and radiators of tracker produce heat that should be removed by tracker  
 407 thermal cooling system (TTCS). TTCS is a two phase CO<sub>2</sub> cooling system with four cooling  
 408 pumps. Due to the ageing and technique problems, the original four pumps were replaced  
 409 by four new pumps in several space walks conducted from November 2019 to January 2020.

410 **3.4. TOF**

411 AMS-02 has 4 planes of Time of Flight (TOF) counters, plane 1 and 2 are above the magnet  
412 (Upper TOF) and plane 3 and 4 are below the magnet (Lower TOF) [66, 67] . Plane 1, 2  
413 and 4 has 8 plastic scintillator paddles while plane 3 has 10. In upper and lower TOF, two  
414 planes are arrange along X and Y directions respectively, see figure 3.12. To avoid possible  
415 gaps between paddles, there paddles are arranged with a 0.5 cm overlapping. Each paddle  
416 is also equipped with 2 or 3 PMTs at the end of the paddle, so the light signal from the  
417 plastic scintillator paddle can be collected by these PMTs and provide efficient detections.

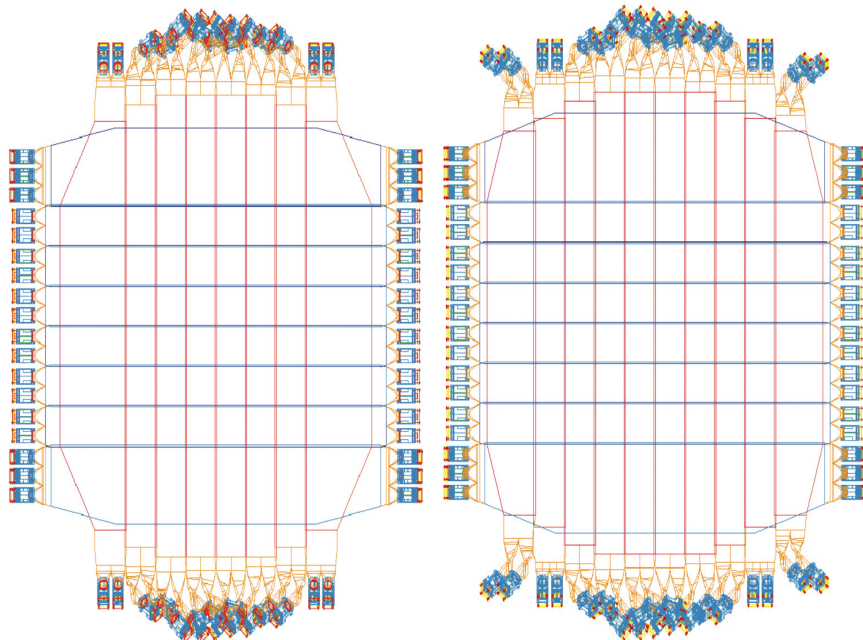
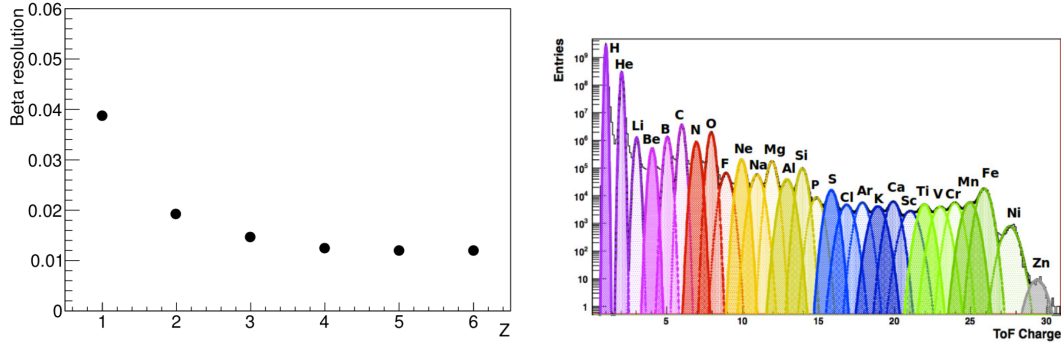


Figure 3.12: TOF planes arrangement in AMS-02 experiment. [68]

418 Combined the information from all the 4 planes, the TOF system can provide the particle  
419 triggers for AMS-02 experiment. More details about trigger will be discussed in 4.7.

420 By measuring the ionisation energy loss  $dE/dX$ , the charge of particles can be obtained from  
421 the anode and dynode of PMTs independently. See figure 3.13(b). The charge resolution is  
422  $\Delta Z = 0.05$  for charge one particle.



(a) TOF Beta resolution as function for particle charge. [68] (b) TOF charge measurement as function of particle charge. [68]

Figure 3.13: AMS-02 TOF beta resolution and charge measurement

423 Except from measuring charge, TOF can also get the velocity of the particle by measuring  
 424 the time differences between upper and lower TOF. Each counter's time resolution is around  
 425 160 ps, and the combined  $\beta$  resolution is around 4% for  $\beta \approx 1$  and  $Z = 1$  particles. See figure  
 426 3.13(a). This provides the ability of discriminate the up-going and down-going particles.

### 427 3.5. RICH

428 In AMS-02 experiment, the ring imaging cherenkov counter (RICH) is installed below the  
 429 lower TOF and above ECAL. The RICH can measure the velocity and the charge of rela-  
 430 tivistic particles. The RICH is composed of two radiators at the top, an expansion volume  
 431 in the middle, and a PMT plane at the bottom [69, 70]. See figure 3.14. The whole RICH  
 432 has a shape of cone with upper radius of 60 cm and lower radius of 67 cm, the height is 47  
 433 cm.

434 When a charged particle traversing a dielectric radiator with a velocity greater than the  
 435 velocity of light in this material, the particle would emit a cone of cherenkov photons.  
 436 The RICH in AMS-02 experiment has a radiator plane of two non-overlapping radiators.  
 437 The central radiator has 16 sodium fluoride tiles (called NaF) of  $85 \times 85 \times 5\text{mm}^3$  with  
 438 refractive index  $n=1.33$ . Outside of NaF, there are 92 silica aerogel tiles (called Agl) of  
 439  $115 \times 115 \times 25\text{mm}^3$  with refractive index  $n=1.05$  [69].

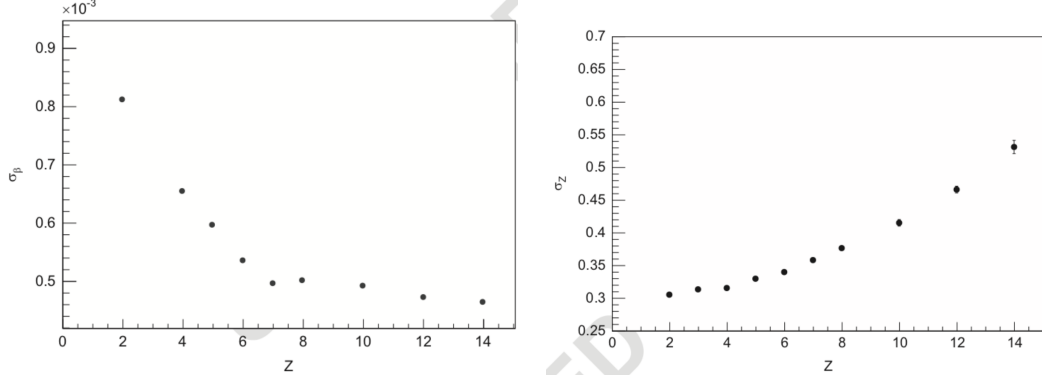


Figure 3.14: RICH PMT plane and expansion volume in front and two radiators in behind. [71]

440 To emit the cherenkov radiation, the velocity of particle has to surpass the speed of light  
 441 in the radiator. Since  $\beta = v/c$  and  $n = c/v$ , this leads to the requirement that particles of  
 442  $\beta > 0.75$  for NaF and particles of  $\beta > 0.953$  for Agl can emit radiation.

443 To increase the detection efficiency, the expansion volume is surrounded by highly reflective  
 444 mirror. The PMT detection plane is equipped with 680 PMT tubes of  $4 \times 4$  multi anodes. The  
 445 effective spatial granularity is  $8.5 \times 8.5\text{mm}^2$ . The opening angle of the cherenkov radiation  
 446 cone  $\theta = \arccos(1/n\beta)$ .

447 The velocity resolution of RICH is  $\sigma_\beta/\beta \approx 10^{-3}$  for charge one particle, see figure 3.15(a).  
 448 The charge measurement of RICH provide a resolution better than 0.5 for particles of charge  
 449 up to 12, see figure 3.15(b).



(a) RICH Beta resolution as function for particle charge. [72] (b) RIICH charge resolution as function of particle charge. [72]

Figure 3.15: RICH beta and charge resolution

### 450 3.6. ECAL

451 The Electromagnetic Calorimeter (ECAL) in AMS-02 experiment provides the ability to  
 452 precisely measure the two profile of longitude and latitude of the electromagnetic shower  
 453 and also the deposited energy [73, 74]. It has a lead-scintillating fiber sandwich structure  
 454 with an active area of  $648 \times 648\text{mm}^2$ , a thickness of 166mm and weight of  $\approx 500$  kg. In total,  
 455 the ECAL has 98 lead foils and 50000 scintillating fibers, the radiation lengths is around 17.

456 The ECAL consists of 9 superlayers with thickness of 18.5 mm. Each superlayer is made  
 457 of 11 grooved lead foils alternate with ten fiber layers glued together with optical epoxy  
 458 (see figure 3.16) [75], while the last superlayer is made of aluminum. Also one superlayer  
 459 is placed along one direction only. By alternatively stacking the 9 superlayers in X and Y  
 460 directions, the 3D image of shower shape is obtained (five on X direction and four on Y  
 461 direction). Each superlayer is readout by 36 PMTs at only one edge. To avoid dead zone  
 462 the PMTs are arranged alternatively. In total, the ECAL has 324 PMTs, 1296 nodes [76].

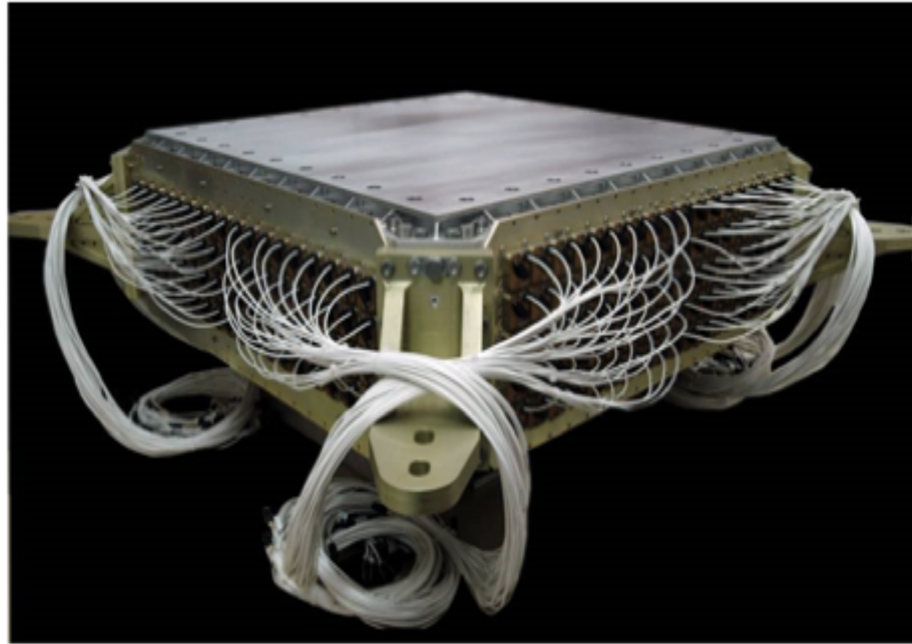


Figure 3.16: ECAL super layer. [54]

463 When a particle goes through the ECAL, it would interact in electromagnetic or hadronicdal  
464 way to produce a shower [77] . An electromagnet shower is made of electrons and positrons  
465 while a hadronic shower are mostly pions and kaons by interacting or decay. Therefore the  
466 hadronic shower looks like wider and more likely to be irregular.

467 The energy resolution has been determined by beam test [78] and can be described by [79]  
468 :

$$\frac{\sigma(E)}{E} = \frac{(10.4 \pm 0.2)\%}{\sqrt{E(GeV)}} \oplus (1.4 \pm 0.1)\% \quad (3.2)$$

469 In figure 3.17, the comparison between measured data and the function is given.

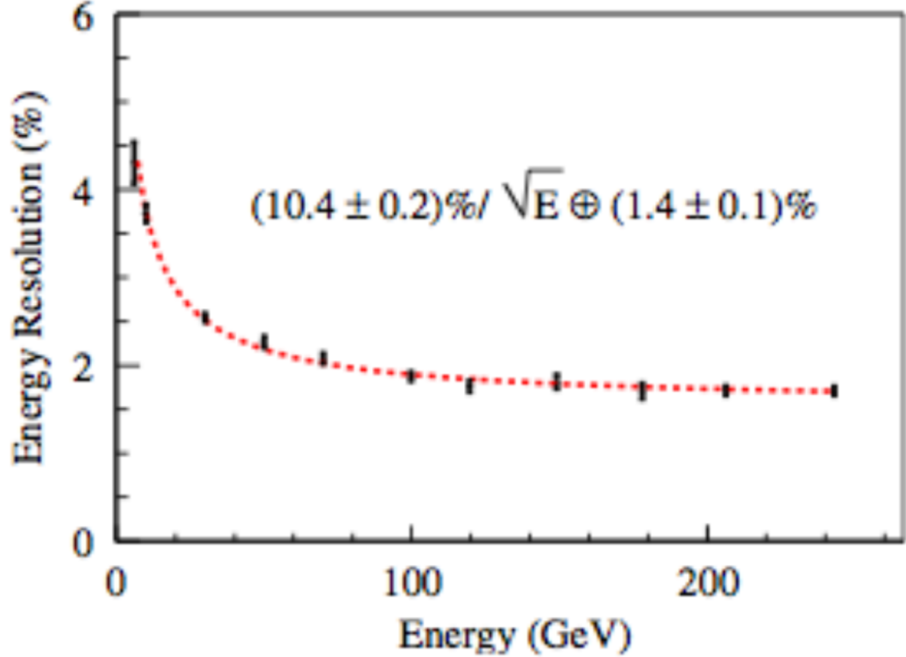


Figure 3.17: ECAL energy resolution [79]

### 470 3.7. ACC

471 The Anti-Coincidence Counters (ACC) in AMS-02 experiment is installed surrounding the  
 472 inner tracker inside the magnet bore [80, 81] , see figure 3.18 upper left one. The first  
 473 purpose is to reject unwanted events like particles entering AMS-02 from side or secondary  
 474 interacting with the sub-detectors. Second task for the ACC is to reduce the trigger rate  
 475 when the ISS going through the area overwhelmingly dominant by low energy large flux like  
 476 SAA [82] .

477 The ACC has a cylinder shape of 1.1 m diameter and 0.83 m height. It is composed of 16  
 478 scintillator panels (Bicron BC-414) with 8 mm thickness, see upper right figure in 3.18. When  
 479 the particles traverse the ACC panels, the particle would emit photon by ionisation energy  
 480 loss in the scintillators. Then the light would be absorbed by the fibers (WLS, Kuraray  
 481 Y-11(200)M) that are embedded into the panels, transported to PMTs (Hamamatsu R5946)  
 482 at the end.

483 A pair of panels is connected to two same PMTs via clear fibers, see figure 3.18 lower one.  
 484 The design is to have some redundancies and also save weight. The slot between these two  
 485 panels has a tongue and groove structure to minimise the inefficiency of detections. After  
 486 the integration of sub-detectors in 2008, the efficiency of panels is determined at CERN  
 487 using muons to be 99.99% [54].

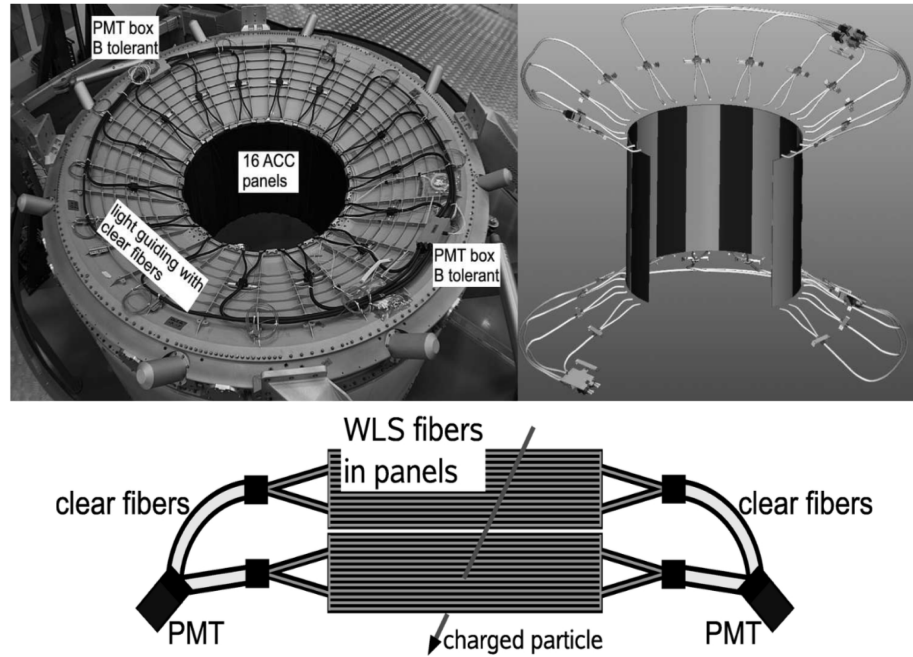


Figure 3.18: Upper left: ACC counter system. Upper right: principle of arrangement. Lower: Panel pair and PMTs connections. [83]

## BIBLIOGRAPHY

- 746 [1] NobelPrize.org (Nobel Media AB). Victor F. Hess - Facts, 2022. URL:  
 747 <https://www.nobelprize.org/prizes/physics/1936/hess/facts>.
- 748 [2] NobelPrize.org (Nobel Media AB). Carl D. Anderson - Facts, 2022. URL:  
 749 <https://www.nobelprize.org/prizes/physics/1936/anderson/facts>.
- 750 [3] NobelPrize.org (Nobel Media AB). The Nobel Prize in Physics 1959, 2022. URL:  
 751 <https://www.nobelprize.org/prizes/physics/1959/summary>.
- 752 [4] Kenneth Greisen. End to the Cosmic-Ray Spectrum? *Phys. Rev. Lett.*, 16:748–750,  
 753 Apr 1966. DOI: [10.1103/PhysRevLett.16.748](https://doi.org/10.1103/PhysRevLett.16.748).
- 754 [5] G T Zatsepin and V A Kuz'min. Upper Limit of the Spectrum of Cosmic Rays.  
 755 *Soviet Journal of Experimental and Theoretical Physics Letters*, 4:78, 8 1966. URL:  
 756 <https://www.osti.gov/biblio/4515382>.
- 757 [6] R. L. Workman and Others (Particle Data Group). Review of Particle Physics. *PTEP*,  
 758 2022:p.083C01, 2022. DOI: [10.1093/ptep/ptac097](https://doi.org/10.1093/ptep/ptac097).
- 759 [7] Alessandra Pacini. Cosmic rays: Bringing messages from the sky to the Earth's surface.  
 760 *Revista Brasileira de Ensino de Fisica*, 39, 01 2017. DOI: [10.1590/1806-9126-RBEF-2016-0168](https://doi.org/10.1590/1806-9126-RBEF-2016-0168).
- 762 [8] W. Baade and F. Zwicky. Cosmic Rays from Super-novae. *Proceedings of the National Academy of Sciences of the United States of America*, 20(5):259–263, 1934. URL:  
 763 <http://www.jstor.org/stable/86841>.
- 765 [9] Massimo Turatto. *Classification of Supernovae*, pages 21–36. Springer Berlin Heidelberg, Berlin, Heidelberg, 2003. DOI: [10.1007/3-540-45863-8\\_3](https://doi.org/10.1007/3-540-45863-8_3).
- 767 [10] Stephen P. Reynolds. Supernova Remnants at High Energy. *Annual Review of Astronomy and Astrophysics*, 46(1):89–126, 2008. DOI: [10.1146/annurev.astro.46.060407.145237](https://doi.org/10.1146/annurev.astro.46.060407.145237).
- 770 [11] Malcolm S. Longair. *High Energy Astrophysics*. UK: Cambridge University Press, 2011.  
 771 URL: <https://ui.adsabs.harvard.edu/abs/2011hea..book....L>.
- 772 [12] ENRICO Fermi. On the Origin of the Cosmic Radiation. *Phys. Rev.*, 75:1169–1174,  
 773 Apr 1949. DOI: [10.1103/PhysRev.75.1169](https://doi.org/10.1103/PhysRev.75.1169).
- 774 [13] T. Gold, F. G. Smith, and A. W. Wolfendale. Pulsars and the Origin of Cosmic  
 775 Rays and Discussion]. *Philosophical Transactions of the Royal Society of London. Series A, Mathematical and Physical Sciences*, 277(1270):453–461, 1975. URL:  
 776 <https://doi.org/10.1080/1364285701270453>.

- 777        <http://www.jstor.org/stable/74493>.
- 778 [14] Bednarek, W. and Bartosik, M. Cosmic rays from Galactic pulsars. *A&A*, 423(2):405–  
779 413, 2004. DOI: [10.1051/0004-6361:20047005](https://doi.org/10.1051/0004-6361:20047005).
- 780 [15] J Arons. Pulsar wind nebulae as cosmic pevatrons: A current sheet’s tale. *Space Sci  
781 Rev*, 173:341–367, 2012. DOI: [10.1007/s11214-012-9885-1](https://doi.org/10.1007/s11214-012-9885-1).
- 782 [16] A. R. Bell. Cosmic ray acceleration in pulsar-driven supernova remnants. *Monthly  
783 Notices of the Royal Astronomical Society*, 257(3):493–500, 08 1992. DOI: [10.1093/mnras/257.3.493](https://doi.org/10.1093/mnras/257.3.493).
- 785 [17] Dan Hooper, Pasquale Blasi, and Pasquale Dario Serpico. Pulsars as the sources of  
786 high energy cosmic ray positrons. *Journal of Cosmology and Astroparticle Physics*,  
787 2009(01):025, jan 2009. DOI: [10.1088/1475-7516/2009/01/025](https://doi.org/10.1088/1475-7516/2009/01/025).
- 788 [18] R. Cowsik. Positrons and Antiprotons in Galactic Cosmic Rays. *Annual Review of  
789 Nuclear and Particle Science*, 66(1):297–319, 2016. DOI: [10.1146/annurev-nucl-102115-044851](https://doi.org/10.1146/annurev-nucl-102115-044851).
- 791 [19] Jan Heisig. Cosmic-ray antiprotons in the ams-02 era: A sensitive probe of dark matter.  
792 *Modern Physics Letters A*, 36(05):2130003, 2021. DOI: [10.1142/S0217732321300032](https://doi.org/10.1142/S0217732321300032).
- 793 [20] Martin Wolfgang Winkler. Cosmic ray antiprotons at high energies. *Journal of Cos-  
794 mology and Astroparticle Physics*, 2017(02):048–048, feb 2017. DOI: [10.1088/1475-7516/2017/02/048](https://doi.org/10.1088/1475-7516/2017/02/048).
- 796 [21] Rolf Kappl and Martin Wolfgang Winkler. The cosmic ray antiproton background for  
797 AMS-02. *Journal of Cosmology and Astroparticle Physics*, 2014(09):051–051, sep 2014.  
798 DOI: [10.1088/1475-7516/2014/09/051](https://doi.org/10.1088/1475-7516/2014/09/051).
- 799 [22] Andrew W. Strong, Igor V. Moskalenko, and Vladimir S. Ptuskin. Cosmic-Ray Propa-  
800 gation and Interactions in the Galaxy. *Annual Review of Nuclear and Particle Science*,  
801 57(1):285–327, 2007. DOI: [10.1146/annurev.nucl.57.090506.123011](https://doi.org/10.1146/annurev.nucl.57.090506.123011).
- 802 [23] Igor V. Moskalenko. Galprop: modeling cosmic ray propagation and associated inter-  
803 stellar emissions, 2011. DOI: [10.48550/ARXIV.1105.4921](https://doi.org/10.48550/ARXIV.1105.4921).
- 804 [24] David Maurin. usine: Semi-analytical models for Galactic cosmic-ray prop-  
805 agation. *Computer Physics Communications*, 247:106942, 2020. DOI:  
806 [10.1016/j.cpc.2019.106942](https://doi.org/10.1016/j.cpc.2019.106942).
- 807 [25] Carmelo Evoli, Daniele Gaggero, Andrea Vittino, Giuseppe Di Bernardo, Mattia Di  
808 Mauro, Arianna Ligorini, Piero Ullio, and Dario Grasso. Cosmic-ray propagation  
809 with DRAGON2: I. numerical solver and astrophysical ingredients. *Journal of Cos-*

- 810        *mology and Astroparticle Physics*, 2017(02):015–015, feb 2017. DOI: [10.1088/1475-7516/2017/02/015](https://doi.org/10.1088/1475-7516/2017/02/015).
- 811
- 812 [26] E. N. Parker. Dynamics of the Interplanetary Gas and Magnetic Fields. *Astrophysical Journal*, 128:664, Nov 1958. DOI: [10.1086/146579](https://doi.org/10.1086/146579).
- 813
- 814 [27] Christopher T. Russell. The Solar Wind and Magnetospheric Dynamics. In *Correlated Interplanetary and Magnetospheric Observations*, pages 3–47, Dordrecht, 1974. Springer Netherlands. DOI: [10.1007/978-94-010-2172-2\\_1](https://doi.org/10.1007/978-94-010-2172-2_1).
- 815
- 816
- 817 [28] M.J. Owens and R.J. Forsyth. The Heliospheric Magnetic Field. *Living Rev. Sol. Phys.*, 10, Nov 2013. DOI: [10.12942/lrsp-2013-5](https://doi.org/10.12942/lrsp-2013-5).
- 818
- 819 [29] A. J. Dessler. Solar wind and interplanetary magnetic field. *Reviews of Geophysics*, 5(1):1–41, 1967. DOI: [10.1029/RG005i001p00001](https://doi.org/10.1029/RG005i001p00001).
- 820
- 821 [30] R Cowen. Voyager 1 has reached interstellar space. *Nature*, 2013. DOI: [10.1038/nature.2013.13735](https://doi.org/10.1038/nature.2013.13735).
- 822
- 823 [31] NASA. Solar wind at voyager 1, 2012. Retrieved 16:20, July 20, 2022 from: [https://commons.wikimedia.org/wiki/File:Solar\\_wind\\_at\\_Voyager\\_1.png](https://commons.wikimedia.org/wiki/File:Solar_wind_at_Voyager_1.png).
- 824
- 825 [32] David H. Hathaway. The Solar Cycle. *Living Reviews in Solar Physics*, 7(1):1, Dec 2010. DOI: [10.12942/lrsp-2010-1](https://doi.org/10.12942/lrsp-2010-1).
- 826
- 827 [33] Carsten Jorgensen, Christoffer Karoff, Senthamizh Pavai Valliappan, and Rainer Arlt. Christian Horrebow’s Sunspot Observations – I. Life and Published Writings. *Solar Physics*, 06 2019. DOI: [10.1007/s11207-019-1465-z](https://doi.org/10.1007/s11207-019-1465-z).
- 828
- 829
- 830 [34] Christoffer Karoff, Carsten Jorgensen, Senthamizh Pavai Valliappan, and Rainer Arlt. Christian Horrebow’s Sunspot Observations – II. Construction of a Record of Sunspot Positions. *Solar Physics*, 294, 06 2019. DOI: [10.1007/s11207-019-1466-y](https://doi.org/10.1007/s11207-019-1466-y).
- 831
- 832
- 833 [35] Eddie Ross and William J. Chaplin. The behaviour of galactic cosmic ray intensity during solar activity cycle 24. *Solar Physics*, 294(1):8, January 2019. DOI: [10.1007/s11207-019-1397-7](https://doi.org/10.1007/s11207-019-1397-7).
- 834
- 835
- 836 [36] EA Bogomolov, ND Lubyanaya, VA Romanov, SV Stepanov, and MS Shulakova. A stratospheric magnetic spectrometer investigation of the singly charged component spectra and composition of the primary and secondary cosmic radiation. In *International Cosmic Ray Conference*, volume 1, page 330, 1979.
- 837
- 838
- 839
- 840 [37] R. L. Golden, S. Horan, B. G. Mauger, G. D. Badhwar, J. L. Lacy, S. A. Stephens, R. R. Daniel, and J. E. Zipse. Evidence for the existence of cosmic-ray antiprotons. *Phys. Rev. Lett.*, 43:1196–1199, Oct 1979. DOI: [10.1103/PhysRevLett.43.1196](https://doi.org/10.1103/PhysRevLett.43.1196).
- 841
- 842

- 843 [38] M. Nozaki. BESS-Polar. *Nuclear Instruments and Methods in Physics Research*  
844 *Section B: Beam Interactions with Materials and Atoms*, 214:110–115, 2004. DOI:  
845 [10.1016/j.nimb.2003.08.005](https://doi.org/10.1016/j.nimb.2003.08.005).
- 846 [39] T. Yoshida, A. Yamamoto, and J. et al. Mitchell. Bess-polar experiment. *Life sciences*  
847 *and space research*, 33(10):1755–1762, 2004. DOI: [10.1016/j.asr.2003.05.017](https://doi.org/10.1016/j.asr.2003.05.017).
- 848 [40] K. Abe et al. Measurement of the cosmic-ray low-energy antiproton spectrum with  
849 the first BESS-Polar Antarctic flight. *Physics Letters B*, 670(2):103–108, 2008. DOI:  
850 [10.1016/j.physlettb.2008.10.053](https://doi.org/10.1016/j.physlettb.2008.10.053).
- 851 [41] K. Abe et al. Measurement of the Cosmic-Ray Antiproton Spectrum at Solar Minimum  
852 with a Long-Duration Balloon Flight over Antarctica. *Phys. Rev. Lett.*, 108:051102,  
853 Jan 2012. DOI: [10.1103/PhysRevLett.108.051102](https://doi.org/10.1103/PhysRevLett.108.051102).
- 854 [42] A M Galper et al. The PAMELA experiment: a decade of Cosmic Ray Physics in  
855 space. *Journal of Physics: Conference Series*, 798:012033, jan 2017. DOI: [10.1088/1742-6596/798/1/012033](https://doi.org/10.1088/1742-6596/798/1/012033).
- 857 [43] O. Adriani et al. (PAMELA Collaboration). New Measurement of the Antiproton-to-  
858 Proton Flux Ratio up to 100 GeV in the Cosmic Radiation. *Phys. Rev. Lett.*, 102:051101,  
859 Feb 2009. DOI: [10.1103/PhysRevLett.102.051101](https://doi.org/10.1103/PhysRevLett.102.051101).
- 860 [44] O. Adriani et al. (PAMELA Collaboration). PAMELA Results on the Cosmic-Ray An-  
861 tiproton Flux from 60 MeV to 180 GeV in Kinetic Energy. *Phys. Rev. Lett.*, 105:121101,  
862 Sep 2010. DOI: [10.1103/PhysRevLett.105.121101](https://doi.org/10.1103/PhysRevLett.105.121101).
- 863 [45] O. Adriani et al. Measurement of the flux of primary cosmic ray antiprotons with  
864 energies of 60-MeV to 350-GeV in the PAMELA experiment. *Pisma Zh. Eksp. Teor.*  
865 *Fiz.*, 96:693–699, 2012. DOI: [10.1134/S002136401222002X](https://doi.org/10.1134/S002136401222002X).
- 866 [46] M. Aguilar et al. (AMS Collaboration). Antiproton Flux, Antiproton-to-Proton Flux  
867 Ratio, and Properties of Elementary Particle Fluxes in Primary Cosmic Rays Measured  
868 with the Alpha Magnetic Spectrometer on the International Space Station. *Phys. Rev.*  
869 *Lett.*, 117:091103, Aug 2016. DOI: [10.1103/PhysRevLett.117.091103](https://doi.org/10.1103/PhysRevLett.117.091103).
- 870 [47] S. et al. Ahlen. An antimatter spectrometer in space. *Nuclear Instruments and Methods*  
871 *in Physics Research Section A: Accelerators, Spectrometers, Detectors and Associated*  
872 *Equipment*, 350(1):351–367, 1994. DOI: [10.1016/0168-9002\(94\)91184-3](https://doi.org/10.1016/0168-9002(94)91184-3).
- 873 [48] Roberto Battiston. The antimatter spectrometer (AMS-02): A particle physics detector  
874 in space. *Nuclear Instruments and Methods in Physics Research Section A: Accelera-*  
875 *tors, Spectrometers, Detectors and Associated Equipment*, 588(1):227–234, 2008. DOI:  
876 [10.1016/j.nima.2008.01.044](https://doi.org/10.1016/j.nima.2008.01.044).

- 877 [49] M Aguilar et al. The Alpha Magnetic Spectrometer (AMS) on the International Space  
878 Station: Part I - results from the test flight on the space shuttle. *Physics Reports*,  
879 366(6):331–405, 2002. DOI: [10.1016/S0370-1573\(02\)00013-3](https://doi.org/10.1016/S0370-1573(02)00013-3).
- 880 [50] Roskosmos. STS-91 PLB, 1998. Retrieved 16:20, July 20, 2022 from:  
881 [https://commons.wikimedia.org/wiki/File:STS-91\\_PLB.jpg](https://commons.wikimedia.org/wiki/File:STS-91_PLB.jpg).
- 882 [51] NASA/Crew-2. View of the iss taken during crew-2 flyaround  
883 (iss066-e-081311), 2021. Retrieved 16:20, July 20, 2022 from:  
884 [https://commons.wikimedia.org/wiki/File:View\\_of\\_the\\_ISS\\_taken\\_during\\_Crew-2\\_flyaround\\_\(ISS066-E-081311\).jpg](https://commons.wikimedia.org/wiki/File:View_of_the_ISS_taken_during_Crew-2_flyaround_(ISS066-E-081311).jpg).
- 886 [52] Zoe Budrikis. A decade of AMS-02. *Nature Reviews Physics*, 3(5):308–308, Jan 2021.  
887 DOI: [10.1038/s42254-021-00320-7](https://doi.org/10.1038/s42254-021-00320-7).
- 888 [53] Fabian Machate. *Study for large acceptance electron analysis with the Alpha Magnetic  
889 Spectrometer on the International Space Station*. Dissertation, RWTH Aachen University,  
890 Aachen, 2021. DOI: [10.18154/RWTH-2021-09976](https://doi.org/10.18154/RWTH-2021-09976).
- 891 [54] AMS Collaboration. The Alpha Magnetic Spectrometer on the International Space  
892 Station, 2022. URL: <https://ams02.space>.
- 893 [55] V. L. Ginzburg and I. M. Frank. Radiation of a uniformly moving electron due to its  
894 transition from one medium into another. *J. Phys. (USSR)*, 9:353–362, 1945.
- 895 [56] M. Heil et al. Operations and Alignment of the AMS-02 Transition Radiation Detector.  
896 In *33rd International Cosmic Ray Conference*, page 1232, 2013. URL:  
897 <https://galprop.stanford.edu/elibrary/icrc/2013/papers/icrc2013-1232.pdf>.
- 898 [57] T. Siedenburg. The AMS TRD. A gasdetector designed for operation in  
899 space. *Nuclear Physics B - Proceedings Supplements*, 150:30–33, 2006. DOI:  
900 [10.1016/j.nuclphysbps.2004.06.001](https://doi.org/10.1016/j.nuclphysbps.2004.06.001).
- 901 [58] Thomas Kirn. The AMS-02 TRD on the international space station. *Nuclear Instruments  
902 and Methods in Physics Research Section A: Accelerators, Spectrometers, Detectors  
903 and Associated Equipment*, 706:43–47, 2013. DOI: [10.1016/j.nima.2012.05.010](https://doi.org/10.1016/j.nima.2012.05.010).
- 904 [59] Jerzy Neyman, Egon Sharpe Pearson, and Karl Pearson. Ix. On the problem of the  
905 most efficient tests of statistical hypotheses. *Philosophical Transactions of the Royal Society  
906 of London. Series A, Containing Papers of a Mathematical or Physical Character*,  
907 231(694-706):289–337, 1933. DOI: [10.1098/rsta.1933.0009](https://doi.org/10.1098/rsta.1933.0009).
- 908 [60] B. Blau, S.M. Harrison, H. Hofer, S.R. Milward, J.S.H. Ross, S.C.C. Ting, J. Ulbricht,  
909 and G. Viertel. The superconducting magnet of ams-02. *Nuclear Physics B - Proceedings  
910 Supplements*, 113(1):125–132, 2002. DOI: [10.1016/S0920-5632\(02\)01831-5](https://doi.org/10.1016/S0920-5632(02)01831-5).

- 911 [61] K. Lubelsmeyer et al. Upgrade of the Alpha Magnetic Spectrometer (AMS-02) for  
 912 long term operation on the International Space Station (ISS). *Nuclear Instruments and*  
 913 *Methods in Physics Research Section A: Accelerators, Spectrometers, Detectors and*  
 914 *Associated Equipment*, 654(1):639–648, 2011. DOI: [10.1016/j.nima.2011.06.051](https://doi.org/10.1016/j.nima.2011.06.051).
- 915 [62] Pierre Erwan Saouter. Operation and Performance of AMS-02 Silicon Tracker. *PoS*,  
 916 Vertex2014:028, 2015. DOI: [10.22323/1.227.0028](https://doi.org/10.22323/1.227.0028).
- 917 [63] Sadakazu Haino. Performance of the AMS-02 silicon tracker in the ISS mission. *Nucl.*  
 918 *Instrum. Meth. A*, 699:221–224, 2013. DOI: [10.1016/j.nima.2012.05.060](https://doi.org/10.1016/j.nima.2012.05.060).
- 919 [64] G. Ambrosi et al. Alignment of the AMS-02 Silicon Tracker. In  
 920 *33rd International Cosmic Ray Conference*, page 1260, 2013. URL:  
 921 <https://ui.adsabs.harvard.edu/abs/2013ICRC...33..570A>.
- 922 [65] B. Alpat et al. The internal alignment and position resolution of the ams-02 sili-  
 923 con tracker determined with cosmic-ray muons. *Nuclear Instruments and Methods in*  
 924 *Physics Research Section A: Accelerators, Spectrometers, Detectors and Associated*  
 925 *Equipment*, 613(2):207–217, 2010. DOI: [10.1016/j.nima.2009.11.065](https://doi.org/10.1016/j.nima.2009.11.065).
- 926 [66] V. Bindi et al. Calibration and performance of the AMS-02 time of flight detector in  
 927 space. *Nucl. Instrum. Meth. A*, 743:22–29, 2014. DOI: [10.1016/j.nima.2014.01.002](https://doi.org/10.1016/j.nima.2014.01.002).
- 928 [67] V. Bindi, A. Contin, N. Masi, A. Oliva, F. Palmonari, L. Quadrani, and A. Tiseni. The  
 929 time of flight detector of the AMS-02 experiment on the international space station.  
 930 *Nucl. Instrum. Meth. A*, 718:478–480, 2013. DOI: [10.1016/j.nima.2012.11.061](https://doi.org/10.1016/j.nima.2012.11.061).
- 931 [68] V. Bindi, E. Choumilov, A. Contin, N. Masi, A. Oliva, F. Palmonari, L. Quad-  
 932 rani, and Q. Yan. The AMS-02 Time of Flight (TOF) System: Construction  
 933 and Overall Performances in Space. In *International Cosmic Ray Conference*, vol-  
 934 ume 33 of *International Cosmic Ray Conference*, page 2298, January 2013. URL:  
 935 <https://ui.adsabs.harvard.edu/abs/2013ICRC...33.2298B>.
- 936 [69] Hu Liu, J. Casaus, F. Giovacchini, A. Oliva, and X. Xia. The RICH detector of  
 937 AMS-02: 5 years of operation in space. *Nucl. Instrum. Meth. A*, 876:5–8, 2017. DOI:  
 938 [10.1016/j.nima.2016.12.011](https://doi.org/10.1016/j.nima.2016.12.011).
- 939 [70] R. Pereira. The AMS-02 RICH detector: Performance during ground-based data taking  
 940 at CERN. *Nucl. Instrum. Meth. A*, 639:37–41, 2011. DOI: [10.1016/j.nima.2010.09.036](https://doi.org/10.1016/j.nima.2010.09.036).
- 941 [71] F. Giovacchini, J. Casaus, and A. Oliva. The AMS-02 RICH detector: Status and  
 942 physics results. *Nuclear Instruments and Methods in Physics Research Section A: Ac-*  
 943 *celerators, Spectrometers, Detectors and Associated Equipment*, 952:161797, 2020. DOI:  
 944 [10.1016/j.nima.2019.01.024](https://doi.org/10.1016/j.nima.2019.01.024).

- 945 [72] F. Giovacchini. Performance in space of the AMS-02 RICH detector. *Nuclear Instruments and Methods in Physics Research Section A: Accelerators, Spectrometers, Detectors and Associated Equipment*, 766:57–60, 2014. DOI: [10.1016/j.nima.2014.04.036](https://doi.org/10.1016/j.nima.2014.04.036).
- 948 [73] Sylvie Rosier-Lees. Performance of the AMS02 electromagnetic calorimeter in space. *J. Phys. Conf. Ser.*, 404:012034, 2012. DOI: [10.1088/1742-6596/404/1/012034](https://doi.org/10.1088/1742-6596/404/1/012034).
- 950 [74] M. Vecchi et al. The electromagnetic calorimeter of the AMS-02 experiment. In *Semaine de l’Astrophysique Francaise (SF2A 2012)*, Nice, France, Jun 2012. URL: <http://hal.in2p3.fr/in2p3-00745677>.
- 953 [75] C. Adloff et al. The AMS-02 lead-scintillating fibres Electromagnetic Calorimeter. *Nucl. Instrum. Meth. A*, 714:147–154, 2013. DOI: [10.1016/j.nima.2013.02.020](https://doi.org/10.1016/j.nima.2013.02.020).
- 955 [76] Marco Incagli. Performance of the AMS-02 Electromagnetic Calorimeter in Space. *PoS, TIPP2014:025*, 2014. DOI: [10.22323/1.213.0025](https://doi.org/10.22323/1.213.0025).
- 957 [77] Manuela Vecchi, Kaiyuan Wu, and Yuan-Hann Chang. A 3-dimensional electromagnetic shower characterization and its application to AMS-02 pointing capability. In *33rd International Cosmic Ray Conference*, page 0653, 2013.
- 960 [78] Stefano Di Falco. Results of 2007 test beam of AMS-02 Electromagnetic Calorimeter. *Adv. Space Res.*, 45:112–122, 2010. DOI: [10.1016/j.asr.2009.08.005](https://doi.org/10.1016/j.asr.2009.08.005).
- 962 [79] G Gallucci and (for the AMS-02 ECAL group). Performance of the AMS-02 Electromagnetic Calorimeter in Space. *Journal of Physics: Conference Series*, 587:012028, feb 2015. DOI: [10.1088/1742-6596/587/1/012028](https://doi.org/10.1088/1742-6596/587/1/012028).
- 965 [80] Ph. von Doetinchem, W. Karpinski, Th. Kirn, K. Luebelsmeyer, St. Schael, and M. Wlochal. The AMS-02 Anticoincidence Counter. *Nucl. Phys. B Proc. Suppl.*, 197:15–18, 2009. DOI: [10.1016/j.nuclphysbps.2009.10.025](https://doi.org/10.1016/j.nuclphysbps.2009.10.025).
- 968 [81] T. Bruch and W. Wallraff. The Anti-Coincidence Counter shield of the AMS tracker. *Nucl. Instrum. Meth. A*, 572:505–507, 2007. DOI: [10.1016/j.nima.2006.10.376](https://doi.org/10.1016/j.nima.2006.10.376).
- 970 [82] A. Basili, V. Bindi, D. Casadei, G. Castellini, A. Contin, A. Kounine, M. Lolli, F. Palmonari, and L. Quadrani. The TOF-ACC flight electronics for the fast trigger and time of flight of the AMS-02 cosmic ray spectrometer. *Nucl. Instrum. Meth. A*, 707:99–113, 2013. DOI: [10.1016/j.nima.2012.12.089](https://doi.org/10.1016/j.nima.2012.12.089).
- 974 [83] Ph. von Doetinchem, Th. Kirn, K. Luebelsmeyer, and St. Schael. The Anticoincidence Counter System of AMS-02, 2009. DOI: [10.48550/ARXIV.0906.1068](https://arxiv.org/abs/0906.1068).
- 976 [84] J.D. Sullivan. Geometric factor and directional response of single and multi-element particle telescopes. *Nuclear Instruments and Methods*, 95(1):5–11, 1971. DOI:

978      [10.1016/0029-554X\(71\)90033-4](https://doi.org/10.1016/0029-554X(71)90033-4).

979    [85] Tim Adye. Unfolding algorithms and tests using RooUnfold. In *PHYSTAT 2011*, pages  
980        313–318, Geneva, 2011. CERN. DOI: [10.5170/CERN-2011-006.313](https://doi.org/10.5170/CERN-2011-006.313).

981    [86] G. D'Agostini. A multidimensional unfolding method based on Bayes' theorem. *Nu-  
982        clear Instruments and Methods in Physics Research Section A: Accelerators, Spectrom-  
983        eters, Detectors and Associated Equipment*, 362(2):487–498, 1995. DOI: [10.1016/0168-9002\(95\)00274-X](https://doi.org/10.1016/0168-984        9002(95)00274-X).

985    [87] Nikolas Zimmermann. *Precision measurement of the cosmic-ray electron and positron  
986        fluxes as a function of time and energy with the Alpha Magnetic Spectrometer on the  
987        International Space Station*. Dissertation, RWTH Aachen University, Aachen, 2020.  
988        DOI: [10.18154/RWTH-2020-02650](https://doi.org/10.18154/RWTH-2020-02650).

989    [88] AMS Collaboration. The Alpha Magnetic Spectrometer (AMS) on the international  
990        space station: Part II – Results from the first seven years. *Physics Reports*, 894:1–116,  
991        2021. DOI: [10.1016/j.physrep.2020.09.003](https://doi.org/10.1016/j.physrep.2020.09.003).